Soft Matter

PAPER

View Article Online
View Journal | View Issue

Cite this: *Soft Matter*, 2024, **20**, 103

Branched copolymer surfactants impart thermoreversible gelation to LAPONITE® gels†

Abhishek Rajbanshi,[abc] Marcelo Alves Da Silva,[b] Najet Mahmoudi,[d] Agnieszka Janeczek,[e] Allison Shaw,[e] Jonathan Dawson[ef] and Michael Thomas Cook *[a]

This investigation seeks to integrate LAPONITE® clay gels with thermoresponsive branched copolymer surfactants (BCSs) to develop advanced functional materials with temperature-induced sol–gel behaviour. It is known that a diverse range of molecules adsorb strongly to clays which may be used to control liberation of the species in healthcare applications, and as such the development of polymer/clay hybrid materials which can add function to the native clay behaviour are of great interest. BCS were synthesised with a structure that encompasses poly(ethylene glycol)methacrylate (PEGMA), ethylene glycol dimethacrylate (EGDMA), and dodecanethiol (DDT), conferring versatile and tuneable thermoresponsive attributes. Systematic modulation of the monomer : DDT/initiator ratio was used to facilitate the synthesis of BCS architectures spanning a range of molecular weights. Through application of small-amplitude oscillatory shear (SAOS) rheology and small-angle neutron scattering (SANS) in conjunction with controlled temperature variations, the sol–gel transition dynamics of these nanocomposite materials were elucidated. Complementary insights into the mechanisms underpinning this transition and temperature-induced alterations in the constituents are gleaned through the utilization of SANS techniques employing contrast-matching methodologies to mitigate clay and polymer scattering interference. It is found that heating systems from room- to body- temperature induces self-assembly of BCS in the bulk aqueous phase with concurrent structuration of clay in gel-forming samples with lower number average molecular weight (M_n). SANS study unpicks this phenomenon to find that gelation occurs with concurrent aggregation of BCS in the bulk, inducing clay–clay interactions only in lower M_n BCS systems with large nanoaggregates.

Received 23rd September 2023,
Accepted 26th November 2023

DOI: 10.1039/d3sm01271a

rsc.li/soft-matter-journal

Introduction

Synthetic nanoclays include the hectorite LAPONITE®™ RD, herein referred to as "LAPONITE®", which has the empirical formula $(Na_{0.7}Si_8Mg_{5.5}Li_{0.3}O_{20}(OH)_4)$.[1] Laponite, a smectite clay, is a layered hydrous lithium magnesium silicate belonging to (2 : 1) phyllosilicates built up of sheets of octahedrally coordinated magnesium oxide between two parallel sheets of tetrahedrally coordinated silica.[2] Once LAPONITE® is dispersed in water, it forms a colloidal dispersion of charged disk-shaped nanoparticles, of thickness *ca.* 1 nm and diameter *ca.* 25 nm.[2] Negative charge on these disks – arising from isomorphic substitutions of lithium for magnesium in the octahedral layer, is distributed at the face, whilst a partial positive charge occurs at the edges.[3] In a single disk the number of positive charges on the edges is approximately 10% of the number of negative charges on the faces, giving LAPONITE® an overall negative charge.[4] At concentrations above ~2 wt% aqueous dispersions of LAPONITE® self-assemble to generate thixotropic arrested gel states driven by particle repulsion. These glassy states transition into attractive gel networks *via* face-edge aggregation in response to changes in salt concentration or pH of the solution.[5] Clays have historical use in pharmaceuticals and cosmetics, for example as sorbents and rheology modifiers, and have gained increased interest due to their ability to control liberation of bioactive proteins.[6] As such, recent developments have led to their exploitation in tissue engineering and biofabrication.[7]

[a] *UCL School of Pharmacy, University College London, London, WC1N 1AX, UK. E-mail: a.rajbanshi@ucl.ac.uk, michael.t.cook@ucl.ac.uk; Tel: +44 (0)2077535800*
[b] *School of Life and Medical Sciences, University of Hertfordshire, Hatfield, AL10 9AB, UK. E-mail: m.da-silva2@herts.ac.uk*
[c] *Institute of Pharmaceutical Science, King's College London, London, SE1 9NH, UK*
[d] *ISIS Muon and Neutron Source, Rutherford Appleton Laboratory, Harwell, Oxford, Didcot OX11 0QX, UK. E-mail: najet.mahmoudi@stfc.ac.uk*
[e] *Renovos Biologics Ltd, Science Park, 2 Venture Rd, Chilworth, Southampton, SO16 7NP, UK. E-mail: agnieszka.janeczek@renovos.co.uk, allison.shaw@renovos.co.uk, JID@soton.ac.uk*
[f] *Institute of Developmental Sciences, Faculty of Medicine, University of Southampton, Southampton, SO16 6YD, UK*

† Electronic supplementary information (ESI) available. See DOI: https://doi.org/10.1039/d3sm01271a

Clay gels can be reinforced with polymers to give composite materials of modulated rheology. Poly(ethylene oxide), for example, is known to adsorb to LAPONITE® clays and increase the elasticity of the system.[8,9] This approach can also induce new phenomena at select concentrations and molecular weight of polymer, such as the production of "shake gels" in which the gel phase occurs only after application of shear. It has been shown that the clays may be combined with stimuli-responsive polymers to give nanocomposite materials with innate advantages of each component.[10,11] Particularly, the response to temperature has shown to impart desirable behaviours to clay gels. For example, Sun and Raghavan demonstrated that mixtures of pluronic F127, a poly(ethylene oxide)$_{99}$-*b*-poly(propylene oxide)$_{65}$-*b*-poly(ethylene oxide)$_{99}$ copolymer, with LAPONITE® gave a material which exhibited sol–gel transition temperature (T_{gel}), switching from a low viscosity Newtonian fluid to gel state when heated above 65 °C.[12] This effect has also been seen in composites of clay with poly(lactide-*co*-glycolide)–poly(ethylene oxide)–poly(lactide-*co*-glycolide)[13] or poly(lactide-*co*-glycolide)–poly(ethylene oxide)[14] (T_{gel} 30–80 °C), as well as poly(2-methyl-2-oxazoline)-*b*-poly(2-*n*-propyl-2-oxazine) (T_{gel} 15 °C).[15]

Branched copolymer surfactants (BCSs) have been demonstrated to enable pH-dependent sol–gel transitions in emulsion systems by Weaver and co-workers.[16–18] In these systems, a BCS containing poly(methacrylic acid) was demonstrated to effectively stabilise oil-in-water emulsions and gave rise to sol–gel behaviours through switching pH from below the pK_a (sol) to above the pK_a (gel). The gel phase in this system was believed to be supported by co-operative H-bonding between BCS allowing droplet–droplet interaction to form a gel phase. Recently, branched copolymer surfactants containing thermoresponsive components with a lower critical solution temperature (LCST) have been shown to form emulsions with sol–gel transition upon heating.[19–21] The advantage of this system is that the BCS, unlike many block copolymer architectures, may be produced in a single pot under scalable conditions using the "Strathclyde approach",[22] simply requiring the monomers and initiators to undergo nitrogen purge and heating in ethanol, a sustainable solvent.[23,24] The synthetic approach allows control of many factors in the thermoresponsive BCS, which is composed of an LCST-imparting monomer, poly(ethylene glycol)methacrylate (PEGMA); ethylene glycol dimethacrylate (EGDMA), as a cross-linker to induce branching, and dodecanethiol (DDT), as a chain transfer agent to impart C12 terminal groups.[19,24] Resultant BCS structures impart varied and controllable thermoresponsive behaviours to oil-in-water emulsions,[21] including the induction of gelation upon heating, however their utility for alternative dispersions, such as clays, has not been explored. Considering the structural similarity of the PEGMA component to poly(ethylene oxide), the potential that BCS will interact with clays was considered as a positive attribute in their selection for composite materials. The BCS architecture has several advantages over the competing systems, giving a one-pot scalable synthesis without the need for anhydrous conditions or heavy metals. The process is capable of routinely producing *ca.* >40 g of material on a lab scale and the composition of the polymer is easily modified by changing the feed monomers. As such, the BCS system has demonstrated great versatility with a range of feed materials.[24–26]

The formation of nanocomposite materials from LAPONITE® and thermoresponsive BCSs has been explored to generate new advanced functional materials. BCS architectures were produced composed of diethylene glycol methyl ether methacrylate (DEGMA), PEGMA, EGDMA, and DDT, with control of monomer : DDT/initiator ratio to give a range of molecular weights. Thermoresponsive behaviour has been explored by small-amplitude oscillatory shear (SAOS) rheology to identify materials which exhibit a sol–gel transition at a physiologically relevant range to allow *in situ* gelation on contact with the body's temperature. The mechanisms underpinning this transition have been explored by small-angle neutron scattering (SANS) with temperature, using contrast-matching techniques to selectively obscure scattering from clays and polymer, elucidating temperature effects on both components.

Materials and methods

Materials

Di(ethylene glycol) methyl ether methacrylate (DEGMA, 95%), poly(ethylene glycol) methyl ether methacrylate (PEGMA, M_n 950 g mol^{-1}), ethylene glycol dimethacrylate (EGDMA, 98%), 1-dodecanethiol (DDT, 99%), D_2O (99.9 atom% D) and anhydrous dodecane (99%) were purchased from Sigma-Aldrich (UK). Alpha, alpha-azoisobutyronitrile (AIBN, >99%) was obtained from Molekula (UK). Ethanol and dimethylformamide (DMF) were supplied by VWR (UK). LAPONITE®-RD was provided by BYK (Germany). Lithium bromide (99%) was purchased from Acros Organics (UK). Dialysis tubing with molecular weight cut off (MWCO) of 14 kg mol^{-1} was purchased from Sigma Aldrich (UK). GPC EasiVial poly(methyl methacrylate) mixed standards were procured from Agilent (UK). Deionised H_2O was employed in all experiments. All chemicals were used as received.

Synthesis of PDEGMA-*co*-PEGMA branched copolymer surfactant by free radical polymerisation

A library of BCS was synthesised according to the feed given in Table 1. DEGMA (174 mmol), PEGMA (6 mmol), EGDMA (12 mmol) and DDT (Table 1) were dissolved in 190 mL ethanol with constant stirring and bubbled with a nitrogen line for 1 h. A solution of AIBN (quantity in Table 1) in 10 mL was then added to the solution. The stirred reaction was then heated to 70 °C for 48 h for polymerisation to complete. After 48 h, the crude product was isolated by distillation to remove ethanol.

Table 1 Reagent quantities for the synthesis of BCS **1–4**

Sample ID:	DEGMA (mmol)	PEGMA (mmol)	EGDMA (mmol)	DDT (mmol)	AIBN (mmol)
1	174	6	12	12	1.2
2	174	6	12	8	0.8
3	174	6	12	6	0.6
4	174	6	12	3	0.3

The resultant crude polymer was then dissolved in water and transferred to a pre-soaked dialysis bag. The dialysis bag was immersed in a beaker containing de-ionised water for 7 to 10 days and the water was replaced at regular intervals (every 1 h for the first 6 h, then at 9 am and 5 pm the following days) to facilitate the purification process. The resultant polymer solution was subjected to lyophilisation for 48 h to obtain the product, which was typically a transparent viscous liquid. The yields for all the lyophilised polymers were 85, 85, 85, and 84% for BCS **1–4**, respectively.

Characterisation of thermoresponsive BCSs

^{1}H NMR was conducted on a Bruker Avance AM 600 MHz NMR instrument with $CDCl_3$ as a solvent at ambient temperature. The residual solvent peak was used as an internal standard. 16 scans were acquired. Data handling was conducted on MestreNova.

The number average molecular weight (M_n) and polydispersity index ($Đ$) of **1–4** were determined using an Agilent 1260 Infinity II GPC equipped with a refractive index (RI) detector. The system was equipped with 2 × Agilent Varian PLGel 5 μm mixed D column. 0.1% w/v lithium bromide in dimethylformamide was used as the eluent, at a flow rate of 0.8 mL min^{-1} with the column temperature set at 30 °C. The system was calibrated with Agilent Easivial poly(methyl methacrylate) (PMMA) standards with M_n ranging from 370 to 364 000 g mol^{-1} (R^2: 0.9998). All samples were prepared in dimethylformamide at a concentration of 2 mg mL^{-1} prior to analysis.

Preparation of BCS/clay composites

Clay was added to deionised water to a concentration of 3 wt% with stirring until a clear dispersion was formed. The sample was then stored at room temperature overnight. This ageing led to a gel mesophase which did not flow under gravitational force. 10 wt% BCS was then slowly added to this mixture with vigorous stirring until dissolution and the sample was stored overnight at room temperature prior to analysis. At the point of analysis, all samples were clear solutions.

Rheology of BCS/clay composites

Rheological measurements were performed on an AR 1500ex rheometer (TA instruments, USA) equipped with a Peltier temperature control unit and a 40 mm parallel plate geometry with a specified gap distance of 500 μm at an oscillating stress of 0.8 Pa and frequency of 6.283 rad s^{-1} (within the linear viscoelastic region of laponite, which yields at >40 Pa).[27] The change in storage modulus (G') and loss modulus (G'') as a function of temperature was recorded and the loss tangent ($\tan\delta$) calculated as G''/G'. Temperature ramps were performed in the range 20 to 60 °C at 1 °C per minute heating/cooling rate. Frequency sweeps were conducted at 20 and 50 °C between 0.5 and 10 rad s^{-1} at a fixed shear stress of 0.8 Pa.

Small-angle neutron scattering

SANS experiments were conducted on the time-of-flight diffractometer instrument SANS2d at the STFC ISIS Neutron and Muon Source (UK). Incident wavelengths from 1.75 to 12.5 Å were used at a sample-to-detector distance of 12 m, which gave a scattering vector (q) range from 1.6 × 10^{-3} to 0.25 Å^{-1}. Temperature of the samples was controlled by an external circulating water bath (Julabo, DE). Samples were loaded in 1 cm wide rectangular quartz cells with 1 mm pathlength. Solutions of 10 wt% BCS and 3 wt% clay were prepared as previously described in either 69% (v/v) D_2O (the remaining volume is H_2O) or 17% (v/v) D_2O (the remaining volume is H_2O). The raw SANS data were then processed using wavelength-dependent corrections to the incident spectrum, detector efficiencies, and measured sample transmissions.[28] The data were then absolutely scaled to give profiles of scattering intensity $I(q)$ as a function of q, using the scattering from a standard sample (comprising a solid blend of protiated and perdeuterated polystyrene) based on established methods.[29] All samples were confirmed to be free of multiple scattering. SANS data were fitted using SASView 4.2.2.[30] Where required, scattering length densities (SLDs) were calculated from the monomeric unit using the Neutron activation and scattering calculator website from NIST centre for neutron research.[31]

For the fitting of SANS data, the scattering intensity $I(q)$ can be written as follows:

$$I(q) = A(P(q)_A S(q)_A) + \text{BKG}$$

where, A is a proportionality constant, BKG is the background, $P(q)$ is the form factor of the scattering object, $S(q)_A$ is the corresponding structure factor when required.

In the case of fitting multiple scattering objects, the expression can be expanded to include further $P(q)$ and $S(q)$ terms. For this work, the BCS/clay mixtures give rise to two scattering signals corresponding to each object, and in some instances a further power-law form factor was required to fit the low q region. Therefore, $I(q)$ is expressed as:

$$I(q) = A(P(q)_A S(q)_A) + B(P(q)_B) + \text{BKG}$$

where, A and B are proportionality constants, BKG is the background, $P(q)_A$ is the form factor for model A, $S(q)_A$ is the corresponding structure factor when required, $P(q)_B$ is the form factor for model B.

$P(q)$ terms used in this study are ellipsoidal, cylindrical, and power law form factors, available in the SASview package and expressed formally elsewhere.[30,32] In the absence of $S(q)$, which contains volume fraction terms, A and B expressed the volume fraction of the scattering object. When the object was believed to be laponite, the volume fraction was determined using the density of laponite. In BCS systems, this was initially approximated using the density of poly(ethylene oxide), such that the weight fraction was approximately equivalent to the volume fraction and fit if required, due to uncertainty in the degree of hydration and density of the BCS. The scattering length density of the solvent systems were calculated and the BKG was approximated by the limit of $I(q)$ at high q. All remaining parameters were fit by the SASview program. When a structure factor was required the inbuilt ''radius_effective_mode'' was set

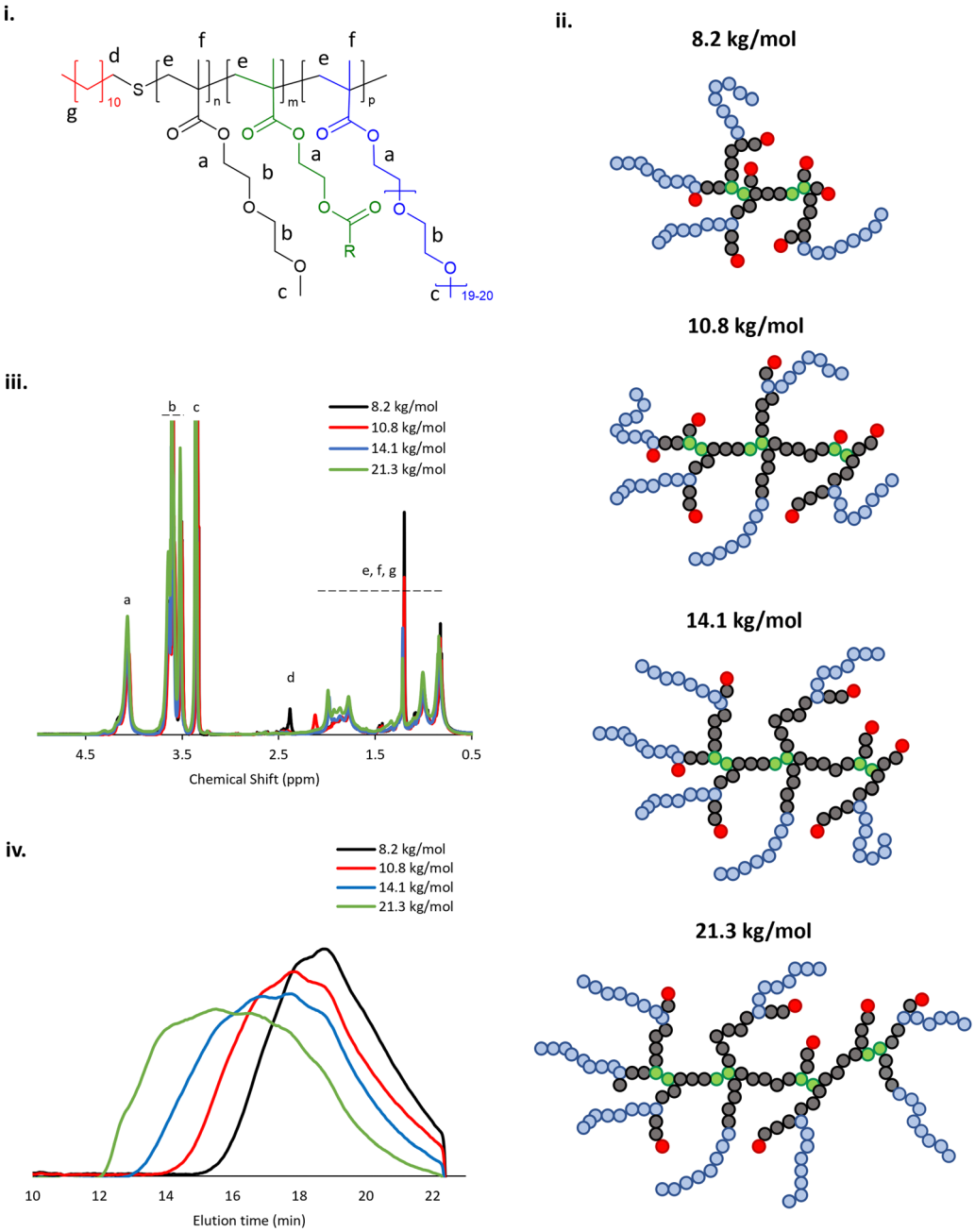

Fig. 1 (i) Simplified chemical structure of the BCS showing hydrophobic alkyl termini (red), thermoresponsive DEGMA (black), hydrophilic PEGMA (blue) and the cross-linking agent (EGDMA) used to induce branching (green). (ii) ^{1}H NMR spectra of the four BCS with varied M_n and (iii) GPC chromatograms. (iv) Schematic representation of BCS showing increase in molecular weight and associated decrease in number of hydrophobic chain ends.

to "average curvature" in the first instance, and unconstrained if required.

Results and discussion

Synthesis of BCS library

The BCS architecture is composed of DEGMA, exhibiting an LCST at *ca.* 27 °C,[33] PEGMA, which acts as a steric stabiliser, EGDMA, which induces branching, and DDT which gives C12 alkyl groups on the polymer termini, imparting surface activity (Fig. 1i). A library of 4 BCS were synthesised and their identities confirmed by ^{1}H NMR, in accordance with prior studies,[20] and GPC (Fig. 1ii, iii). These BCS **1–4** had molecular weights ranging from 8.2 to 21.3 kg mol^{-1}, determined on a narrow calibration relative to poly(methyl methacrylate) (Table 2). During polymerisation, AIBN decomposes on heating to give 2-cyanoprop-2-yl radicals which can initiate chain growth. Homolytic bond fission and concomitant hydrogen abstraction from the thiol moiety of the DDT generates thioyl radicals which transfers the

Table 2 Molecular weights of BCS used in this study

Sample ID:	M_n (kg mol^{-1})	M_w (kg mol^{-1})	$Đ$
1	8.2	18.5	2.3
2	10.8	33.0	3.1
3	14.1	68.3	4.8
4	21.3	180.9	8.5

chain growth to give dodecane-terminated chains. Decreasing the ratio of DDT/AIBN to monomers in the reaction mixture can increase ultimate polymer M_n whilst also reducing the relative abundance of hydrophobic chain ends. The breadth of the molecular weight distributions observed increased with M_n, as shown in Table 2. The proposed structure of samples **1–4** is shown in Fig. 1iv, where the DEGMA and PEGMA copolymerisation will lead to a comb-polymer like structure with a poly(DEGMA) backbone and PEG pendants from the PEGMA inclusion plus dodecyl-end groups from DDT.[20,34,35] EGDMA induces branching in these comb-like systems. It has previously been found that increased M_n favours thermoresponsive gel formation in emulsion systems.[20]

Rheological evaluation of laponite and BCS/laponite composite gels

The rheology of 3 wt% LAPONITE® gels studied SAOS rheology with varied temperature is shown in Fig. 2i. At this small-amplitude, the fluid was predominantly solid-like with tan δ approximately 0.1 across the temperatures studied. The gel was soft, with G' consistently *ca.* 150 Pa across 20–50 °C. The expected structure for this gel mesophase is based on previous studies of LAPONITE® which indicates that the disk-like morphology, bearing negative face charge with positive edge charge (Fig. 2ii), allows the formation of a "house-of-cards" structure (Fig. 2iii) or Wigner glass (Fig. 2iv),[4] an amorphous state stabilized by long-range repulsive interactions.[36] In the absence of any additive, LAPONITE® gels are not thermoresponsive in this temperature range.

The addition of 10 wt% BCS to the LAPONITE® gel imparted several different behaviours to the native nanoclay gel. From initial observation by eye, all materials were freely-flowing transparent liquids at room temperature. Mild heating to 37 °C resulted in turbidity in all samples and the appearance of a homogenous gel-like phase in the 8.2 (**1**) and 10.8 (**2**) kg mol^{-1} BCS/clay mixtures, without any phase separation observed. Of note, the system only exhibited this thermoreversible gelation when clay was dispersed in water prior to addition of BCS. The reverse order of addition did not elicit this response. SOAS temperature ramps were then conducted to evaluate these transitions (Fig. 3). The 8.2 kg mol^{-1} BCS **1**/clay (10/3 wt%) mixture underwent sol–gel transition with T_{gel} occurring at 40 °C. Below this temperature the system was liquid-like

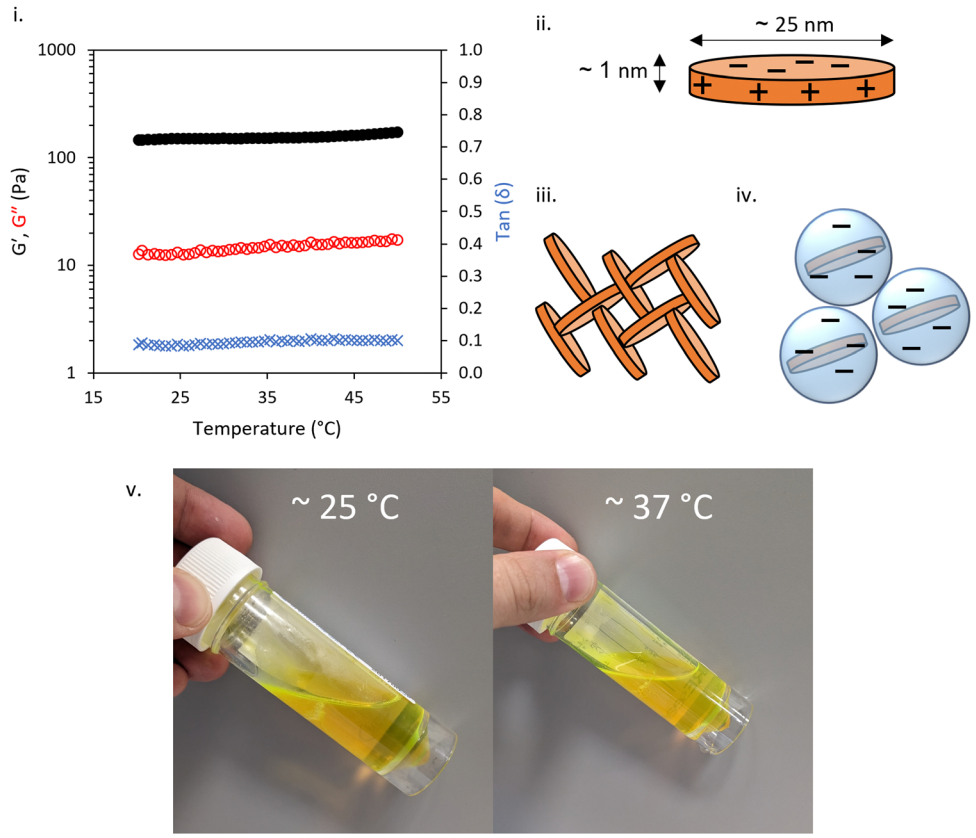

Fig. 2 (i) SAOS temperature ramps of LAPONITE® at 3 wt%. G' and G'' are shown in black and red, respectively, with tan δ given in blue. Rheological analysis conducted at 0.8 Pa and 6.283 rad s^{-1}. (ii) schematic structure of LAPONITE® clay disks, with proposed "house of cards" (iii) and Wigner glass (iv) gel structures. (v) BCS **1** solution showing liquid-like behaviour at 25 and 37 °C. Fluorescein added for clarity of image.

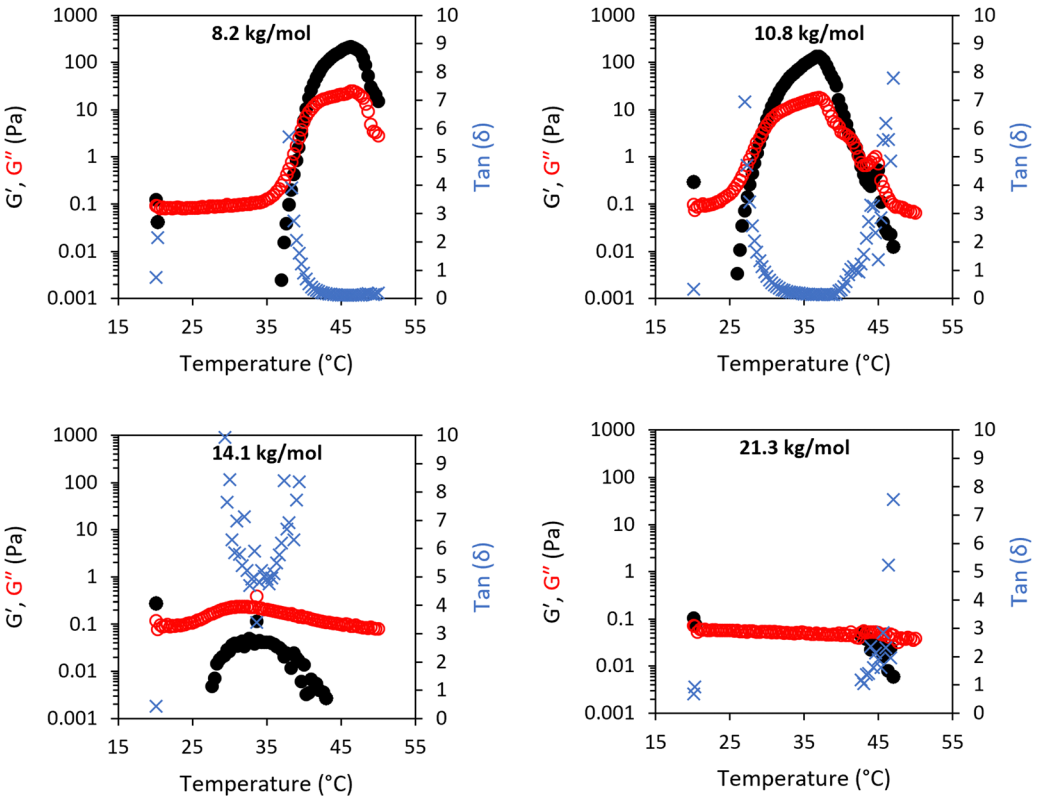

Fig. 3 SAOS temperature ramps of LAPONITE® and BCS composite fluids at 3 at 10 wt%, respectively. The effect of BCS molecular weight was explored (inset). G' and G'' are shown in black and red, respectively, with $\tan\delta$ given in blue.

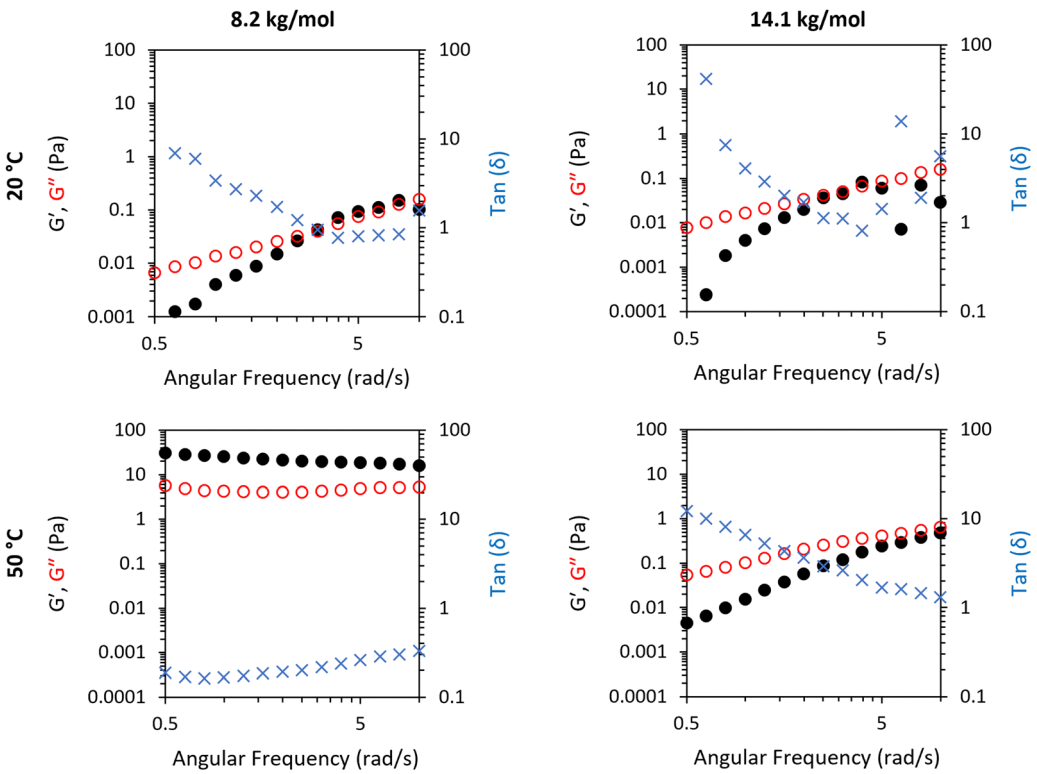

Fig. 4 SAOS frequency sweeps of LAPONITE® and BCS composite fluids at 3 and 10 wt%, respectively. The effect of BCS molecular weight was explored (inset above). G' and G'' are shown in black and red, respectively, with $\tan\delta$ given in blue. Molecular weight (M_n) appears above the figure.

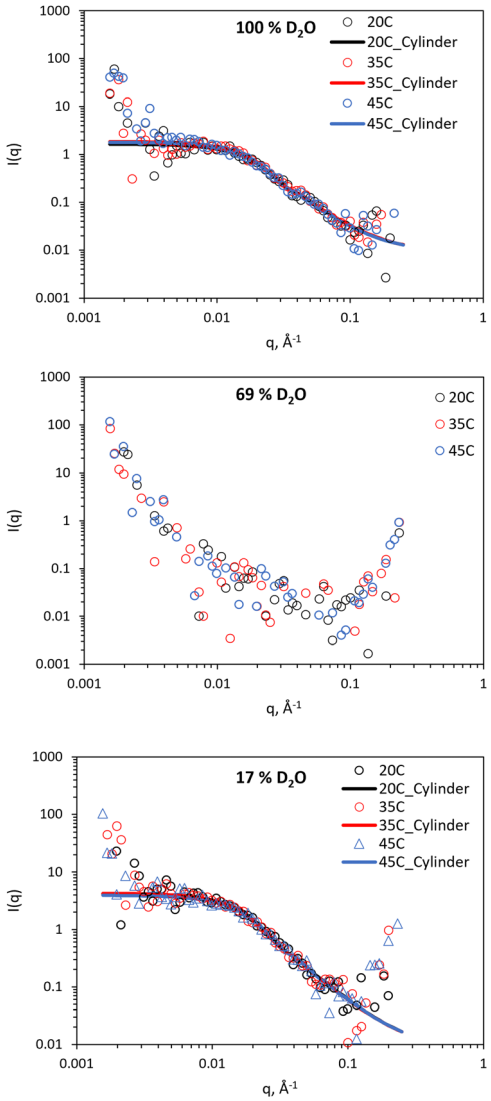

Fig. 5 SANS of 3 wt% LAPONITE® clay at 100, 69, and 17% v/v D_2O (in H_2O), with the latter two contrasts matching out LAPONITE® and polymer, respectively. Lines represent a fit to the data shown as open circles, using the form factor inset. SANS data with error is included in Fig. S1 and S2 (ESI†).

($\tan\delta > 1$) with low viscosity (G'' *ca.* 0.1 Pa). At 40 °C, the material became a predominantly solid-like ($\tan\delta < 1$) soft gel state reaching a G' maxima at 46 °C of 213 Pa. Above T_{gel}, the value of $\tan\delta$ was equivalent to the 3 wt% LAPONITE® gel, having an a value *ca.* 0.11. Above 46 °C, the material began to soften, with G' reducing to 15 Pa at 50 °C. The 10.8 kg mol^{-1} BCS **2**/clay system also exhibited thermoresponsive gelation, with T_{gel} exhibited at 30 °C with a G' maxima of 130 Pa at 37 °C ($\tan\delta$ *ca.* 0.13). Above 42 °C, the reverse transition was observed, with the mixture switching back to a liquid-like state with $\tan\delta > 1$. This softening is proscribed to phase separated domains which appear in the system at elevated temperatures, occurring at lower temperatures as the larger M_n polymer **2**. Neither the 14.1 kg mol^{-1} BCS **3** or 21.3 kg mol^{-1} BCS **4** gave thermoresponsive gelation, but the BCS **3**/clay mixture showed weak thickening event at *ca.* 30–40 °C. By comparison, BCS solutions alone at 10 wt% concentration in water exhibit liquid-like behaviour at both room and body temperature (Fig. 2v). It is known that BCS solutions alone thicken at 20 wt%,[20] however the materials formed are weak, have $\tan\delta > 1$, and the concentrations reported in these clay/BCS composites are below the concentration needed to impart this thickening. Thus, the behaviour of BCS in the bulk alone does not explain the thermoresponsive gelation observed in BCS **1** and **2**.

SAOS frequency sweeps were conducted on two nanoclay mixtures of **1** and **3** to probe the different rheological features of a gel-forming system (**1**) and a non-gel-forming system (**3**), with M_n 8.2 and 14.1 kg mol^{-1}, respectively (Fig. 4). This gave exploration of frequency dependence of G' and G'' on a thermoresponsive gel (**1**/clay) and a non gel-forming mixture (**3**/clay). The **1**/clay mixture exhibited a high frequency dependence of G' and G'' at 20 °C with a dominance of liquid-like behaviour at low frequencies. G' and G'' never exceeded 0.2 Pa. Overall, this indicates the mixture behaved as a weak viscoelastic fluid. Measurement of frequency-dependence was also probed at 50 °C to explore the rheological features above the LCST transition. At 50 °C the material had switched to a stronger gel state, characterised by a low frequency dependence of G' and G'' at elevated absolute values of 20 and 8 Pa. The BCS **3** behaved as a weak viscoelastic fluid at both temperatures studied.

Small-angle neutron scattering study of BCS/LAPONITE® composites

SANS was employed to comprehend nanostructural changes in the BCS/clay mixtures and native clay. Contrast matching was employed to extract information about both constituent materials. In a contrast matching experiment, the variation scattering contrast is achieved through the choice of different molar amounts of isotopic solvents (H_2O/D_2O). If the molar average scattering length density (SLD) of the solvent mixture is equivalent to either the clay or BCS components, the scattering arises only from the unmatched component. This technique therefore allows the determination of the form of individual components in complex mixtures.[37] SANS was conducted under three solvent conditions, namely: 100% D_2O, in which scattering arises from both BCS and clay; 69% (v/v) D_2O (ρ = 1.0759 g cm^{-3}) which is contrast matched to clay (SLD = 4.2 × 10^{-6} Å^{-2}), and 17% (v/v) D_2O (ρ = 1.0187 g cm^{-3}) which is contrast matched to the estimated SLD of the BCS based on poly(ethylene oxide) from a prior publication (0.63 × 10^{-6} Å^{-2}).[37] BCS**1–4**/clay mixtures were evaluated, as well as LAPONITE® alone, at 20, 35 and 45 °C to understand temperature-induced changes to the system, at the same concentration rheology was conducted at (10 wt% BCS/3 wt% LAPONITE®). 20 °C allows study of the sol form of the material at room temperature, 35 °C studies the gel form of **2**/clay, and at 45 °C the gel form of **1**/clay is covered. Focus in the manuscript is on the 17 and 69% v/v contrasts, which were sufficient to study the behaviour of the composites.

The SANS study of the 3 wt% LAPONITE® is shown in Fig. 5, with fitting parameters in ESI.† Signals from scattering can be observed in the 100 and 17% (v/v) D_2O solutions, however no

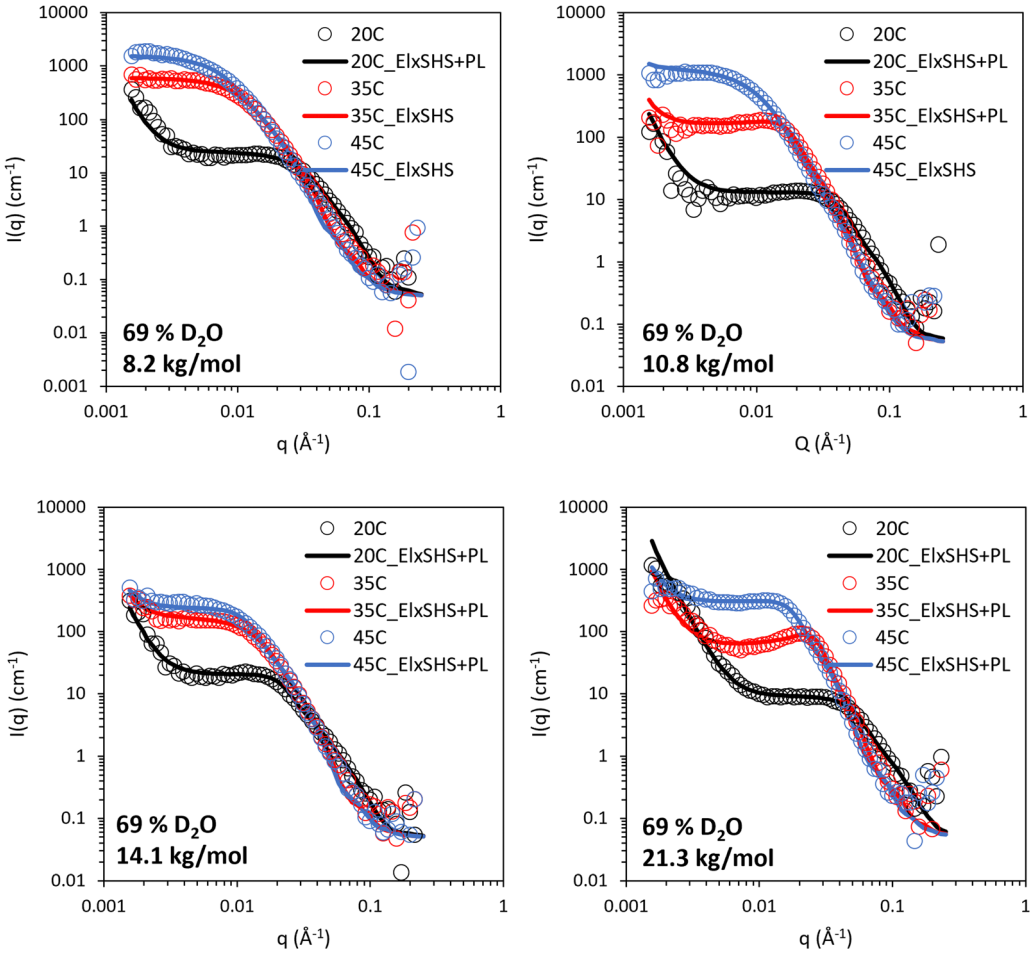

Fig. 6 SANS of 10 wt% BCS/3 wt% LAPONITE® clay in 69% v/v D_2O (in H_2O), calculated to contrast match laponite. Lines represent a fit to the data shown as open circles, using the form factor inset. El: ellipsoid, SHS: sticky hard sphere, PL: power law. SANS data with error is included in Fig. S3–S6 (ESI†).

features are observed in the 69% (v/v) contrast, demonstrating effective masking of the LAPONITE® system. In accordance with the rheological analysis, no substantial change in signal was observed with temperature change. Fitting was conducted with the following parameters fixed: volume fraction (0.0118, assuming a density of LAPONITE® equal to 2530 kg L^{-1}),[3] SLD of scattering object (4.2×10^{-6} $Å^{-2}$, equivalent to LAPONITE®), and SLD of solvent (6.37, 4.22 or 0.62×10^{-6} $Å^{-2}$ for the 100, 69, and 17% (v/v) D_2O contrasts). Background incoherent scattering was estimated from the limit of $I(q)$ at high q. All samples could be fit to a cylindrical form factor of length < diameter, indicative of a disk-like structure, with uniform SLD.[38] The length of the cylinder, which can also be considered the thickness of the disk, was determined to be between 6–7 Å, whilst having a radius of 120–130 Å (Table S1 and S2, ESI†), consistent with prior knowledge that the laponites are *ca.* 1 nm thickness with diameter of 25 nm. The SANS provides not only confirmation of the disk nanostructure, but also affirms that temperature induced no structural changes over the range measured. No correlation peaks were observed and the fitting required no structure factor to be present, providing evidence that there is not close association between the disk forms. The lower limit of q (1.56×10^{-3} $Å^{-1}$) is associated with a distance (d) of *ca.* 4028 Å by the relation $d = 2\pi/q$. Thus, there is no evidence of regular distancing of the disks within this range. It is therefore postulated that the Wigner glass model is more likely than the house of cards structure in this sample, in accordance with studies by Becher *et al.*[4]

The BCS/lapornite composite gels were then studied by SANS under the same three contrasts, *i.e.* 100, 69, and 17% (v/v) D_2O. Initially, the 69% (v/v) D_2O contrast is discussed (Fig. 6), in which the LAPONITE® clay is matched to the solvent and thus and scattering present arises from BCS and BCS supramolecular structures. All systems could be fit to a combination of ellipsoidal form factor with a "sticky hard sphere" structure factor with an additional power law which appears as an upturn at low q. The "sticky hard sphere" model describes particles as hard spheres that can stick together upon contact. The "stickiness" parameter in this model quantifies the strength of the attraction between particles at the point of contact. The low q upturn fit to a q^{-4} power law, indicating the presence of larger objects with smooth interfaces.[39] Parameters for this fitting are included in Tables S4–S6 (ESI†).

The mid-to-high q region (ca $5 \times 10^{-3} < q < 0.1$ $Å^{-1}$) of the BCS/LAPONITE® gels in 69% (v/v) D_2O (Fig. 5) shows features

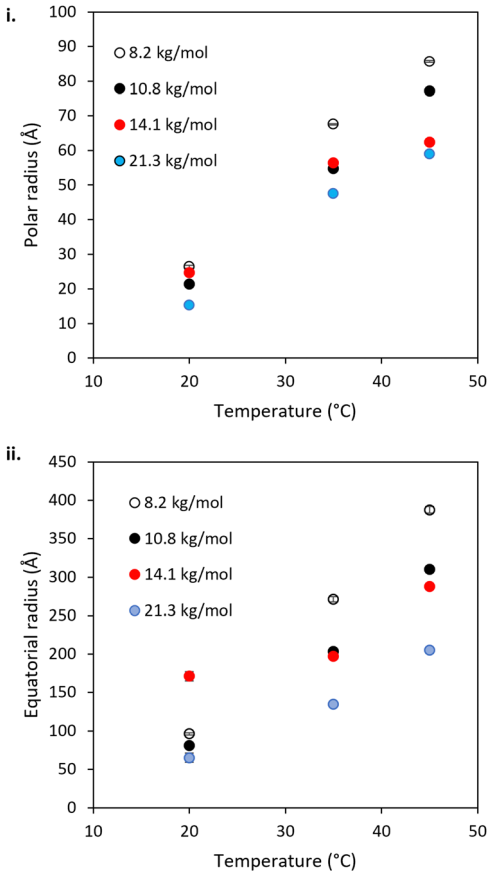

Fig. 7 Polar (i) and equatorial (ii) radii of the BCS aggregates present in 10 wt% BCS/3 wt% LAPONITE® clay in 69% v/v D_2O (in H_2O), extracted from SANS fit. Error bars represent the error in the fitting from SasView.

dominated by the ellipsoidal form factor with a sticky-hard-sphere structure factor. In all systems, the ellipsoidal nano-objects are oblate, having equatorial > polar radii (Fig. 7). This is consistent with prior SANS and TEM study of the BCS solutions in D_2O (in the absence of clay) and thus is believed to indicate the presence of BCS aggregates in the bulk. The oblate geometry is attributed to steric constraints from the branched structure not allowing it to take the required curvature to permit the thermodynamically-preferred spherical morphology often seem in linear micellar systems.[20] In all systems both polar and equatorial radii of the BCS aggregates increased upon heating from 20–45 °C. This is attributed to the increased hydrophobicity of the poly(DEGMA) component of the BCS undergoing LCST transition over this range, driving nanostructural rearrangements for example the aggregation of smaller aggregates into larger ones due to reduced stability on heating. The counterintuitive decrease in these radii with increasing M_n is a likely indicator that the larger M_n polymers form nano-objects with lower aggregation numbers.

The low q region of the BCS/LAPONITE® gels in 69% (v/v) D_2O, *ca.* $q < 5 \times 10^{-3}$, gives an indication of structural features larger than the q range measured by the presence of an upturn, particularly noticeable at 20 °C. The feature is fit to a q^{-4} decay which describes objects with a sharp interface without resolving any dimensions for the scatterer, which in this case are expected to be larger than the limit of low q.[40] The feature is present only at 20 °C in the 8.2 kg mol^{-1} BCS **1**/clay system, disappearing at 35 and 45 °C. Again, the feature is most prominent at 20 °C in the 10.8 kg mol^{-1} BCS **2**/clay sample, and barely detectable at 35 °C. By 45 °C no upturn at low q is observed. The feature remains observable at all temperatures for the 14.1 and 21.3 kg mol^{-1} BCS **3** and **4**/clay composites. Thus, it is believed that in these materials there are additional larger-scale structures unresolvable by SANS at 35 and 45 °C, *i.e.* above LCST of poly(DEGMA).

The 17% v/v D_2O/H_2O contrast was intended to probe the structure of LAPONITE® in polymer/clay composites, where the SLD of this mixture (0.62×10^{-6} $Å^{-2}$) aimed to match that of the PEGMA/DEGMA component of the BCS. The DDT component is expected to have a significantly different SLD (ca -0.37×10^{-6} $Å^{-2}$) so all the components of the BCS cannot be matched in a singled contrast. In BCS **3** (14.1 kg mol^{-1}) solutions alone, no features were observed at 20 °C, with a weak intensity scattering present at 35 and 45 °C which is believed to be due to this DDT component and any small deviations in SLD from expected values for PEGMA/DEGMA (Fig. 8). For the BCS/clay composites there was no evidence of changes to clay structure at 20 °C as the features present could be adequately fit with a disk-type form factor as per the clays without polymer (Fig. 8 and Fig. S9–S12, ESI†). Heating the systems to 35 and 45 °C gave rise to the appearance of increased scattering at low q. The magnitude of this scattering increase was *ca.* 10-fold higher than that seen for the BCS solution alone at the same concentration without clay. This data could not be fit by simple addition of the two individual form factors, which did not give sufficient intensity of the low q feature (ca two-fold lower), or by increased volume fraction of the form factor arising from the BCS aggregates measured in 17% v/v D_2O, which did not fit the mid (q) region (Fig. S13, ESI†). It was possible to fit the data by application of a squarewell structure factor to the disk form factor which describes the scattering from clay. The squarewell model describes particles as hard spheres with an attractive potential extending a finite distance beyond the particle surface, like a "well" around each particle. In addition to hard-core repulsion, it includes a square well potential, where the attractive force between particles is constant over a certain range outside the particle surface and then abruptly drops to zero. This model is suitable for systems where the attractive forces between particles with specific interaction ranges.[30] While this model is strictly designed for spheres it is a reasonable approximation for other particle shapes. It can be seen that the intensity of scattering at low q is dependent upon the molecular weight of BCS, leading to decreased scattering at higher M_n. The 21.3 kg mol^{-1} BCS/clay composite shows scattering only from the clay disk. Assuming this scattering arises from clay–clay interaction, inferred from the presence of the structure factor, then lower M_n more effectively drives intimate contact of the clay nanodisks. This is in-line with rheological experiments which indicated thermoreversible gel formation only in the 8.2 and 10.8 BCS/clay composites. Thus,

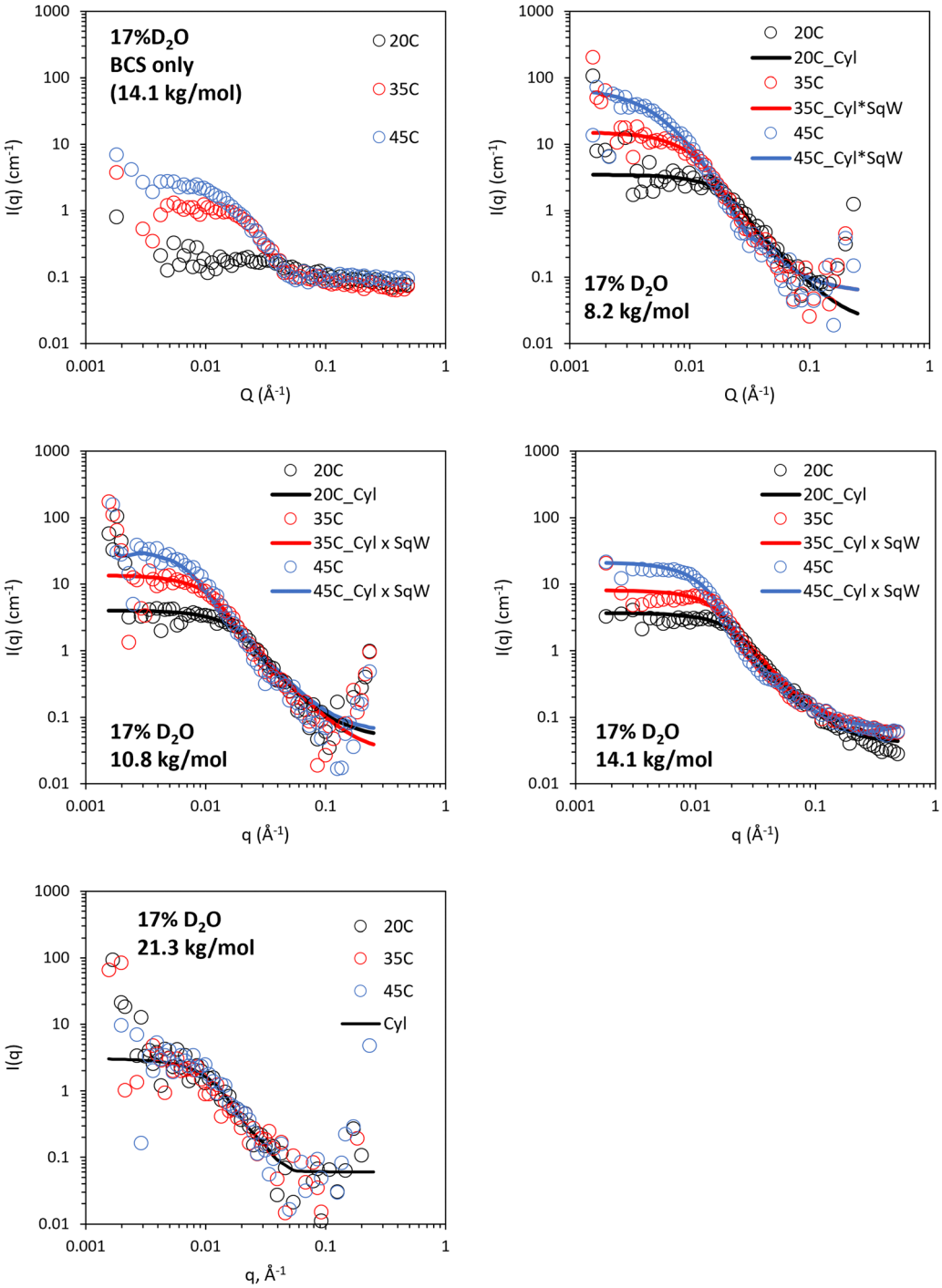

Fig. 8 SANS of 10 wt% BCS/3 wt% LAPONITE® clay in 17% v/v D_2O (in H_2O), calculated to contrast match PEGMA/DEGMA of BCS. Lines represent a fit to the data shown as open circles, using the form factor inset. Cyl: cylinder, SqW: square well. SANS data with error is included in Fig. S9–S12 (ESI†). Parameters from fitting are included in Tables S7–S9 (ESI†).

it is believed that the ability of lower M_n systems to form large aggregates is more effective in driving clay-interactions to form a gel phase. It is also possible that the higher relative abundance of hydrophilic PEG groups to the hydrophobic DDT component renders the higher M_n BCS active on the clay face even above LCST, considering PEG's strong interaction with clays.[9] All samples exhibited an upturn at low q which was not fit due to the high error on the measurements.

Conclusions

BCS impart thermoreversible gelation to LAPONITE® gels in the M_n range 8.2–10.8 kg mol^{-1}, however higher M_n systems did not exhibit this sol–gel switch. These BCS/clay composites may therefore flow freely at room temperature, as opposed to LAPONITE® clay solutions alone, but switch to a gel state when heated to internal body temperature (37 °C). This phenomenon

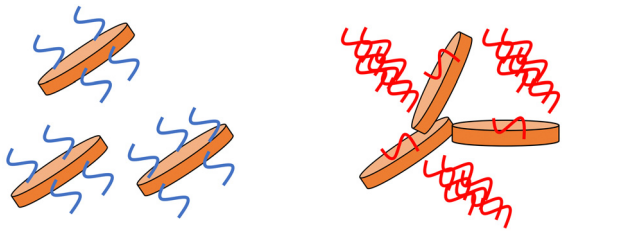

Fig. 9 Simplified schematic showing proposed mechanism for thermoreversible gel formation in BCS/clay composites. Polymer is shown in blue when below LCST, and red when above LCST. LAPONITE® is shown as an orange disk. For clarity the schematic omits factors including the presence of polymer aggregates below LCST and considerations regarding molecular weight effects.

offers new functional materials for exploitation in healthcare technologies, for example as *in situ* gels for injection or topical application. Rheological study was complimented by contrast matching SANS experiments to probe mechanisms underpinning the sol–gel transition. Taking all experiments into account, the following suggestions are made:

– Disruption of gel formation in LAPONITE® clay solutions by BCS indicates interaction of polymer and clay to alter surface characteristics and disrupt formation of Wigner glass state.

– Temperature drives formation of ellipsoidal aggregates of BCS in the bulk for all M_n studied.

– Lower M_n BCS **1** and **2** drive the intimate contact of clays above LCST of DEGMA, allowing gel formation. It is possible that the larger aggregates formed in the 8.2 and 10.8 kg mol^{-1} BCS **1** and **2**/clay composites provide sufficient steric bulk to force contact between LAPONITE® disks. This process is shown as a simplified schematic in Fig. 9.

In comparison with existing thermoreversible clay gels, the BCS system gives the advantage of its scalability and functionality, as well as the transitions exhibited by the composite gels. These materials are typically exploited for *in situ* gelation on heating to physiological temperature, either for drug delivery or cellular applications such as biofabrication, and thus it is desirable for sol–gel transition to occur between room (ca 25 °C) and body (ca 37 °C) temperature. Poloxamer 407/clay materials have been shown to exhibit a gelation temperature of 65 °C, far above that required for healthcare or cellular applications.[12] Poly(oxazoline)/clay materials give this transition at 15 °C, requiring refrigeration to enter the liquid state, thus causing concerns with processing or application in this form.[15] Poly(lactide-*co*-glycolide)–poly(ethylene oxide)–poly(lactide-*co*-glycolide)/clay mixtures give gelation temperature of *ca.* 30–80 °C dependent on concentration, and thus under specific conditions may give the desired *in situ* gelation behaviour.[13,14] However, these materials are costly, hydrolyse in water, and require heavy metal in their synthesis, creating problems for translation. The BCS architecture, in this context, gives an ideal platform for the generation of future polymer/clay composites responding to alternative stimuli as well as defining M_n requirements for sol–gel behaviours.

Future studies are required to further probe ageing effects in these composite materials which are problematic in conventional clay gels. The current study ensured equivalent ageing between samples of 24 h, however temporal effects on the behaviour of the systems are not yet known. The future view for these materials is that they be utilised for bioprinting or healthcare applications, requiring study of cellular compatibility and/or toxicological assay, in addition to performance testing. Furthermore, rheological analysis at the target application temperature is required. Whilst cationic surfactants in particular are known to cause cell lysis, non-ionic polymeric surfactants, like the BCS, have previous utility in pharmaceuticals at high concentrations, for example polysorbate 20 appears in medicines at up to 15 wt%.[41] Future studies will seek to probe compatibility *in vivo* or on 3D culture models where the presence of an epithelial barrier is likely to mitigate the possibility of false positives relative to 2D culture.

Conflicts of interest

Agnieszka Janeczek and Allison Shaw are employees of Renovos Biologics Ltd. Jon Dawson is a co-founder of the company.

Acknowledgements

The Hertfordshire Science Partnership and the EPSRC (EP/T00813X/1) are thanked for funding. The STFC ISIS facility is thanked for awarding access to the SANS2D beamline for neutron scattering experiments (2220037). The Hertfordshire Science Partnership is also acknowledged for supporting the project under the Therapy Accelerator Scheme.

References

1 M. Kroon, W. L. Vos and G. H. Wegdam, *Phys. Rev. E: Stat. Phys., Plasmas, Fluids, Relat. Interdiscip. Top.*, 1998, **57**, 1962–1970.
2 B. Ruzicka and E. Zaccarelli, *Soft Matter*, 2011, **7**, 1268–1286.
3 K. Suman and Y. M. Joshi, *Langmuir*, 2018, **34**, 13079–13103.
4 T. B. Becher, C. B. Braga, D. L. Bertuzzi, M. D. Ramos, A. Hassan, F. N. Crespilho and C. Ornelas, *Soft Matter*, 2019, **15**, 1278–1289.
5 V. Can and O. Okay, *Des. Monomers Polym.*, 2005, **8**, 453–462.
6 J. I. Dawson, J. M. Kanczler, X. B. Yang, G. S. Attard and R. O. C. Oreffo, *Adv. Mater.*, 2011, **23**, 3304–3308.
7 G. Cidonio, M. Glinka, Y. H. Kim, J. M. Kanczler, S. A. Lanham, T. Ahlfeld, A. Lode, J. I. Dawson, M. Gelinsky and R. O. C. Oreffo, *Biofabrication*, 2020, **12**(3), 035010.
8 S. Kishore, S. Srivastava and S. R. Bhatia, *Polymer*, 2016, **105**, 461–471.
9 X. Liu and S. R. Bhatia, *Polym. Adv. Technol.*, 2015, **26**, 874–879.
10 M. Shen, Y. Sun, J. Xu, X. Guo and R. K. Prud'Homme, *Langmuir*, 2014, **30**, 1636–1642.
11 M. A. Da Silva and C. A. Dreiss, *Polym. Int.*, 2015, **65**, 268–279.
12 K. Sun and S. R. Raghavan, *Langmuir*, 2010, **26**, 8015–8020.

13 M. Miyazaki, T. Maeda, K. Hirashima, N. Kurokawa, K. Nagahama and A. Hotta, *Polymer*, 2017, **115**, 246–254.
14 T. Maeda, M. Kitagawa, A. Hotta and S. Koizumi, *Polymers*, 2019, **11**, 250.
15 C. Hu, L. Hahn, M. Yang, A. Altmann, P. Stahlhut, J. Groll and R. Luxenhofer, *J. Mater. Sci.*, 2021, **56**, 691–705.
16 J. V. M. Weaver, S. P. Rannard and A. I. Cooper, *Angew. Chem., Int. Ed.*, 2009, **48**, 2131–2134.
17 R. T. Woodward, L. Chen, D. J. Adams and J. V. M. Weaver, *J. Mater. Chem.*, 2010, **20**, 5228–5234.
18 A. L. B. Maçon, S. U. Rehman, R. V. Bell and J. V. M. Weaver, *Chem. Commun.*, 2016, **52**, 136–139.
19 M. A. Silva, A. Rajbanshi, D. Okopu-Achampong and M. T. Cook, *Macromol. Mater. Eng.*, 2022, 2200321.
20 A. Rajbanshi, M. A. da Silva, D. Murnane, L. Porcar, C. A. Dreiss and M. T. Cook, *Polym. Chem.*, 2022, **13**, 5730–5744.
21 A. Rajbanshi, N. Mahmoudi, D. Murnane, E. Pavlova, M. Slouf, C. A. Dreiss and M. T. Cook, *Int. J. Pharm.*, 2023, **637**, 122892.
22 N. O'Brien, A. McKee, D. C. Sherrington, A. T. Slark and A. Titterton, *Polymer*, 2000, **41**, 6027–6031.
23 K. Tekin, N. Hao, S. Karagoz and A. J. Ragauskas, *ChemSusChem*, 2018, **11**, 3559–3575.
24 R. Baudry and D. C. Sherrington, *Macromolecules*, 2006, **39**, 1455–1460.
25 J. V. M. Weaver, S. P. Rannard and A. I. Cooper, *Angew. Chem.*, 2009, **121**, 2165–2168.
26 L. G. Weaver, R. Stockmann, A. Postma and S. H. Thang, *RSC Adv.*, 2016, **6**, 90923–90933.
27 A. Pek-Ing and L. Yee-Kwong, *Appl. Clay Sci.*, 2015, **107**, 36–45.
28 R. K. Heenan, J. Penfold and S. M. King, *J. Appl. Crystallogr.*, 1997, **30**, 1140–1147.
29 G. D. Wignall and F. S. Bates, *J. Appl. Crystallogr.*, 1987, **20**, 28–40.
30 SasView version 4.2.2, **https://www.sasview.org/2019-05-20-release-4.2.2/**.
31 NIST SLD Calculator, **https://www.ncnr.nist.gov/resources/sldcalc.html**, (accessed 20 April 2021).
32 M. A. da Silva, P. Haddow, S. B. Kirton, W. J. McAuley, L. Porcar, C. A. Dreiss and M. T. Cook, *Adv. Funct. Mater.*, 2022, **32**, 2109010.
33 C. Porsch, S. Hansson, N. Nordgren and E. Malmström, *Polym. Chem.*, 2011, **2**, 1114–1123.
34 J. Bassi, P. Haddow, M. Luciano and M. T. Cook, *J. Mol. Liq.*, 2022, **346**, 117906.
35 M. A. Da Silva, A. Rajbanshi, D. Opoku-achampong, N. Mahmoudi, L. Porcar, P. Gutfreund, A. Tummino, A. Maestro, C. A. Dreiss and M. T. Cook, *Macromol. Mater. Eng.*, 2022, **307**, 2200321.
36 G. Porpora, F. Rusciano, V. Guida, F. Greco and R. Pastore, *J. Phys.: Condens. Matter*, 2021, **33**, 104001.
37 D. C. Pozzo and L. M. Walker, *Colloids Surf., A*, 2004, **240**, 187–198.
38 J. S. Pedersen, *Adv. Colloid Interface Sci.*, 1997, **70**, 171–210.
39 S. M. King, in *Modern Techniques for Polymer Characterisation*, ed. R. A. Pethrick and J. Dawkins, John Wiley & Sons, Ltd, 1999, pp. 171–232.
40 L. A. Feigin and D. I. Svergun, *Structure Analysis by Small-Angle X-Ray and Neutron Scattering*, Springer, New York LLC, 1st edn, 1987.
41 FDA, Inactive Ingredient Database for Approved Drug Products, **https://www.accessdata.fda.gov**, (accessed 4 January 2023).